UNIVERSITY OF OXFORD

OXFORD ASTROPHYSICS

THE NATURE OF THE SUPERSOFT X-RAY SOURCE RX J0513–69

K.A. Southwell, M. Livio, P.A. Charles, D. O'Donoghue
and W.J. Sutherland

Submitted to *The Astrophysical Journal*

Ref: OUAST/96/17

Address: Department of Physics,
Astrophysics,
Keble Road,
Oxford,
OX1 3RH,
England.

Submitted to *The Astrophysical Journal*

The nature of the supersoft X-ray source RX J0513–69

K. A. Southwell[1], M. Livio[2], P. A. Charles[1], D. O'Donoghue[3] and W. J. Sutherland[1]

ABSTRACT

We present spectroscopy and photometry of the LMC supersoft binary system RX J0513.9-6951. We derive a refined spectroscopic period of P= 0.761 ± 0.004 d, which is consistent with the value obtained from long term photometric monitoring (P= 0.76278 ± 0.00005 d). We see bipolar outflow components of HeII and Hβ, with velocities of $\sim 3800\,\mathrm{km\,s^{-1}}$, strongly suggesting that the compact object is a white dwarf. Using all the available optical and X-ray data, we construct a theoretical model to explain the principal features of the unusual variability of this source. In particular, we note that X-ray outbursts have only been seen at times of optical minima. From this, we conclude that the most likely cause of the X-ray outbursts is a photospheric contraction during a nuclear shell burning phase, rather than a thermonuclear flash or shocked emission. The system probably comprises a relatively massive white dwarf accreting at a high rate ($\sim 10^{-6} M_\odot\ \mathrm{yr^{-1}}$) from an evolved donor star, and is observed close to pole-on.

Subject headings: accretion, accretion discs — binaries: spectroscopic — stars: individual (RX J0513.9-6951) — X-rays: stars

1. INTRODUCTION

The supersoft X-ray sources (SSS) are a class of luminous ($L_{\mathrm{bol}} \sim 10^{37} - 10^{38}\,\mathrm{erg\,s^{-1}}$) objects, with a characteristic radiation temperature of $(1 - 10) \times 10^5$ K. Seven such sources are now known in the Galaxy, 11 in the Magellanic Clouds, 15 in M31 and candidates exist also

[1]Dept. of Astrophysics, Nuclear Physics Building, Keble Road, Oxford, OX1 3RH, UK.
E-mail: kas@astro.ox.ac.uk; pac@astro.ox.ac.uk; wjs@astro.ox.ac.uk

[2]Space Telescope Science Institute, 3700 San Martin Drive, Baltimore, MD 21218, USA.
E-mail: mlivio@stsci.edu

[3]Department of Astronomy, University of Cape Town, Rondebosch 7700, South Africa.
Email: dod@uctvms.uct.ac.za

in M101, NGC 253 and M33 (see reviews by Hasinger 1994; Kahabka & Trümper 1996; Cowley et al. 1996).

The most popular theoretical model for the SSS consists of a binary system in which a white dwarf accretes mass from a subgiant companion at such a high rate that it burns hydrogen steadily at its surface (van den Heuvel et al. 1992; Rappaport et al. 1994). The difference between SSS and ordinary cataclysmic variables is in the high accretion rates (by a factor $\sim 100 - 1000$) in the SSS. More recently, Yungelson et al. (1995) have shown that three major binary subpopulations may contribute to the Galactic population of SSS with: (i) low mass main sequence donors, (ii) low mass subgiant donors, and (iii) (super)giant donors.

The transient supersoft source RX J0513.9–6951 (hereafter 0513–69) was discovered in outburst during the ROSAT All Sky Survey (Schaeidt, Hasinger & Trümper 1993). In 1990 October/November the source brightened in X-rays by about a factor of 20 during a period of $\sim$ 10 days. A formal black body fit to the PSPC data gave a temperature of about 40 eV and a bolometric luminosity of $\sim 2 \times 10^{38}\,\mathrm{erg\,s^{-1}}$, for a column density of $N_{\mathrm{H}} = 9.4 \times 10^{20}\,\mathrm{cm^{-2}}$. The source has been monitored roughly every three months between November 1992 and October 1993 and was found to be three times in an off-state and once, on 20/22 July 1993, in an on-state, with a similar brightness to that observed in the first outburst (Schaeidt 1996). Furthermore, a series of weekly HRI pointings between 3 November 1994 and 3 March 1995 revealed a third X-ray outburst around the end of December 1994. A typical turn-on time of $\sim$ 6 d (from survey data) and turn-off time of $\lesssim$ 1 week (from the HRI pointings) were thus proposed for this source by Schaeidt (1996).

This object has been identified with a $\sim$ 17 mag emission-line star in the LMC (Pakull et al. 1993; Cowley et al. 1993). Spectroscopic observations by Crampton et al. (1996), hereafter C96, showed that the spectrum is dominated by He II emission lines and H+HeII blends. Their radial velocity measurements suggested a binary period of 0.76 d, but no orbital photometric variations were found. However, we have recently published a $\sim$ 3 year light curve of 0513–69, from observations made during the MACHO project (Alcock et al. 1996). This photometry revealed a high level of optical variability, including recurrent low states, in which the brightness drops by $\sim$ 1 mag every $\sim 100 - 200$ days. The extended time-base over which these observations were made enabled us to detect an orbital modulation, although of small semi-amplitude ($\sim$ 0.02 mag). The photometric period thus derived, $P = 0.76278 \pm 0.00005$ d, is consistent with the independent spectroscopic result.

In the current work, we present further spectroscopic and photometric observations of 0513–69, in which we see some unusual features, including evidence for high velocity outflows and optical variability on timescales as short as $\sim$ 3 h. We then use all the available optical and X-ray data in an attempt to construct a comprehensive theoretical model for the source. The spectroscopic observations are described in § 2, and the photometry in § 3. In § 4, we present a refined spectroscopic period, and consider the implications of the derived binary parameters and

mass function. A discussion and the proposed model follow.

2. SPECTROSCOPY

2.1. Observations and Reduction

We obtained intermediate resolution spectra of 0513–69 on the nights 29/11/94 – 1/12/94 using the 3.9 m Anglo-Australian Telescope at Siding Spring, Australia. The detector was a Tek CCD attached to the RGO spectrograph, using a 1200V grating. The wavelength coverage is 4367–5070Å in the blue and 6103–6857Å in the red, with a resolution of ~ 1.3 Å. Due to variable cloud and generally poor seeing, no standard stars were observed, hence the spectra are not flux calibrated. Cu-Ar arc spectra were taken at regular intervals for calibration of the wavelength scale in the reduction procedure. A series of tungsten flat fields and bias frames were also obtained. Tab. 1 lists the journal of observations.

The data reduction was performed using the Starlink FIGARO package and PAMELA routines of K. Horne. Removal of the bias signal was achieved through subtraction of the mean overscan level on each frame. This was acceptable since an examination of the bias frames showed no significant structure. Small scale pixel-to-pixel sensitivity variations were removed by multiplying by a balance frame prepared from flat fields of a tungsten lamp. One-dimensional spectra were extracted using the optimal algorithm of Horne (1986), and calibration of the wavelength scale was achieved using the MOLLY package of T. R. Marsh.

2.2. Results and Analysis

We present below the spectroscopic data and give a description of the principal features. A detailed radial velocity analysis is given later in § 4.

We show in Fig. 1 the variance-weighted average of all our blue spectra. HeII and Hβ are seen strongly in emission, with narrow cores and broad bases. Previous spectroscopic observations (Pakull et al. 1993; C96) have shown the presence of highly ionised elements, notably OV (5595 Å), OVI (5290 Å) and NV. Given our limited spectral coverage, we are unable to comment on the presence of oxygen. However, we find marginal evidence for the NV 4603/4619 Å emission lines reported by the latter authors. The spectral region around 4600 – 4700 Å, shows evidence for the Bowen NIII-CIII $\lambda\lambda$ 4640 – 50 Å complex and probable CIV 4658.3Å, although these lines are contaminated by the underlying HeII emission.

In Fig. 2, we present the mean red spectrum, which is dominated by strong Hα emission. Although the signal-to-noise ratio is poor, we are able to identify components (marked S^- and S^+, following the nomenclature of C96) in emission. Similar features are evident on each side of the

HeII 4686Å and Hβ lines in Fig. 1. These unusual features were first noted in the blue by Pakull (1994) and Cowley et al. (1996), and interpreted as high velocity components of HeII and Hβ. Recently, C96 have confirmed this identification, being unable to attribute the lines to any likely ionic species, and concluding an origin in some type of bipolar outflow.

All the spectra were examined for nightly variations in the strength and shape of the emission lines. However, no significant changes were apparent in the major lines over the course of the observing run. In Tab. 2, we list the mean equivalent widths of the major emission features for each night, and also for the overall average red and blue spectra. We give the 1σ statistical errors, although we caution that systematic uncertainties may arise due to the difficulty of assessing the continuum level for broad based line profiles. Also tabulated are the equivalent widths of the S^+/S^- emission components. The wavelengths and relative velocities of the S^+/S^- components, measured from the average spectra of Figs. 1 and 2, are listed in Tab. 3. Our findings are consistent with the measurements of C96, supporting the interpretation of these features as Doppler-shifted components of the HeII and Balmer lines.

We see further evidence for high velocity flows within this system in the emission line profiles of HeII 4686Å and Hβ (see Fig. 1). The former line exhibits a pronounced blue wing, extending to ~ 3800 km s^{-1} (see also C96). Furthermore, the blue side of the Hβ emission appears to be absorbed.

3. PHOTOMETRY

3.1. The Optical Light Curve

0513-69 lies in one of the fields surveyed by the MACHO project (see e.g. Alcock et al. 1995). As a result of this serendipitous photometric monitoring, a record of the optical variability of this source exists from 1992 August to the present time. For completeness, we show in Fig. 3 the MACHO light curve of 0513-69 for the period 1992 Aug. 22 – 1995 Nov. 27. These observations have recently been published in Alcock et al. (1996), to which we refer the reader for further details regarding the data acquisition and reduction, and a discussion of the variability. However, we have also marked on Fig. 3 arrows indicating the times at which the system was known to be definitely on and off in X-rays; we refer to this later in § 5.3 and § 5.4. The optical light curve is dominated by recurrent low states, representing ~ 0.8 mag reductions in intensity, which occur at quasi-regular intervals. In addition, 0513–69 exhibits erratic variability on shorter timescales, with fluctuations of up to ~ 0.3 mags occurring on timescales of days.

We have also obtained white-light photometry of 0513–69 using the SAAO 1 m telescope at Sutherland, South Africa. These observations were made on 1995 Feb. 5 ($\equiv$ JD 2449754 - marked "SAAO" on Fig. 3), at a time when 0513–69 was in an optical high state. The detector was the UCT CCD, operating in frame transfer mode. In this configuration, only half of the chip

is exposed, and at the end of the integration, the signal is read out through the masked half. In this way, we are able to obtain consecutive integrations with virtually no CCD dead time. The effective wavelength of the instrument, in the absence of a filter, is approximately that of the Johnson V passband, but with a bandwidth of $\sim$ 4000Å (FWHM). In Fig. 4, we show the resulting light curve, which consists of 1328 10 s exposures, obtained over a continuous 220 min period. The magnitude of 0513–69 and a comparison star are plotted relative to a local standard. We see a fading in the brightness of 0513–69 of $\sim$ 0.1 mags, which is not observed in the comparison star. Thus, we find evidence that 0513–69 can exhibit significant optical variability on timescales as short as $\sim$ 3 h. We performed a power spectrum analysis of the data, using the method of Scargle (1982). No significant power was revealed within the range of periods to which the search was sensitive ($\sim$ 30 s – 2 hr). By adding an artificial sinusoidal component to the data, we derive an upper limit of $\sim$ 0.015 mags for the semi-amplitude of any real modulation on these short timescales.

4. BINARY PARAMETERS

4.1. The Spectroscopic Period

4.1.1. Measurement of line velocities

We measured the line velocities of HeII 4686 by fitting triple Gaussian functions to the line profiles. These fits consisted of a narrow component for the line core, an underlying broader Gaussian to account for the red emission shoulder and a further wide, low-amplitude component, to fit the extended blue emission wing, which includes the $\lambda\lambda$ 4640 – 50 Å Bowen blend. We list in Tab. 4 the radial velocities of HeII 4686 for our 10 blue spectra, obtained from the strong narrow component. The velocity centroids of the broad components were far less accurately determined, and we do not give these. A triple Gaussian fit to the HeII 4686 profile of the average blue spectrum is shown in Fig. 5.

4.1.2. Period search

The periodogram for HeII 4686 is shown in Fig. 6. The frequency space ranges from 0.1 – 10.0 cycles per day, with a search interval of 0.001 cycles per day (a more wide ranging search failed to reveal further significant power). We have applied the CLEAN algorithm of Roberts, Lehár and Dreher (1987), which essentially deconvolves the spectral window from the data. The major peak is at P= 0.761 $\pm$ 0.025 d, which is entirely consistent with the "best" spectroscopic value of 0.76 d obtained by C96. The power arising at 4.54 d (ν = 0.22 cycles d^{-1}) is considered due to a one day^{-1} alias.

Given the extremely limited sampling of our dataset, we combined our HeII 4686 radial

velocities with those of C96, which were obtained only $\lesssim 3$ weeks before our observations. In order to correct for any systematic differences between the data, we first subtracted the mean value from each set. The CLEANED periodogram, shown in Fig. 7, is dominated by a peak at P= 0.761 ± 0.004 d, with one day^{-1} aliases at $\nu \approx 0.33$ cycles d^{-1} and $\nu \approx 2.30$ cycles d^{-1}.

We therefore confirm the spectroscopic period suggested by C96, and find that this is consistent, within the 1σ errors, with the photometric period of P= 0.76278 ± 0.00005 d (Alcock et al. 1996).

4.2. The Mass Function and Parameter Space

We folded our HeII 4686 radial velocities on P= 0.76278 d (this being the most accurate period determination available) using the photometric ephemeris for the time of maximum optical brightness: T_o = JD 2448857.832(5) + 0.76278(5)E (Alcock et al. 1996). The resulting radial velocity curve is shown in Fig. 8 with a sinusoidal fit. We obtain a velocity semi-amplitude, K= 14.5±3 km s^{-1}, a systemic velocity, γ = 297±1 km s^{-1} and zero crossing phase $\phi_o = 0.17 \pm 0.09$. The error on the latter quantity includes the uncertainty in the photometric ephemeris. We also combined our velocity data with that of C96 (see § 4.1.2 above) and repeated this procedure, although the data were difficult to fit since C96 give no errors. This yielded a zero-crossing phase of 0.30 ± 0.08 and velocity semi-amplitude of $\sim$ 11 km s^{-1}, which are not significantly different from the parameters obtained from our data alone. Given the very low amplitude of the modulation and the intrinsic uncertainty in the photometric ephemeris, we are unable to obtain an accurate value for ϕ_o. Thus, it is difficult to draw conclusions from the relative phasing of the light and velocity curves. However, the data do suggest that at maximum optical light, the velocities are most blue-shifted. Assuming that the HeII arises near the compact object, this could be explained if we are viewing the inner irradiated edge of the disk, near the impact point of the stream.

The mass function for the parameters derived from our data alone is $f(M) = PK^3/2\pi G$ = 0.0002±0.0001 $M_\odot$, which is plotted in Fig. 9 for various inclinations (see also C96). Clearly, if the accretor is a white dwarf, the inclination of the system must be very low, i.e. seen close to pole-on. This conclusion is unaltered for the highest mass function allowed by the uncertainty on the measurement. Whilst it appears statistically unlikely that we are viewing the system close to pole-on ($i \lesssim 7°$), the following points argue for this possibility (see also C96):

(1) If the inclination is not very small (see above), the brightness of the disk would imply unreasonably high accretion rates (in excess of the Eddington limit - see § 5.2).

(2) The orbital photometric variations are extremely small ($\sim$ 0.04 mag full amplitude - see § 1). With a high accretion rate (§ 5.2) and steady burning at the white dwarf surface (§ 5.4), the illuminated hemisphere of the secondary would be expected to produce larger variations at higher inclination angles. For example, the eclipsing SSS, CAL 87, exhibits photometric variations of $\sim$ 0.5 mag (excluding the eclipse) for an inclination of $i \gtrsim 70°$ (Schmidtke et al. 1993; Schandl,

Meyer-Hofmeister & Meyer 1996).

We note that in such a low inclination system, in which the accretor is a white dwarf, the implied mass of the companion star is such that it would not fill its Roche lobe if on the main sequence. An evolved donor star is therefore required.

5. DISCUSSION AND MODEL

We will now discuss the implications of the observations presented here, as well as of other available data, for models of the system.

5.1. The Nature of the Compact Object

The first thing we would like to establish is the nature of the compact object. To this goal, we note that observations of young stellar objects (e.g. Reipurth & Heathcote 1993), of AGN (e.g. Blandford 1993), of SS 433 (e.g. Vermeulen 1993) and of the Galactic black hole candidates GRS 1915+105 (Mirabel & Rodriguez 1994) and GRO 1655-40 (Hjellming & Rupen 1995) *all* indicate that the velocities of jets are always of the order of *the escape velocity from the central object*. The observations presented in § 2 (see also C96) indicate bipolar outflows or jet speeds of $V_{\rm bipolar} \sim 3800\,{\rm km\,s^{-1}}$. If interpreted as an escape velocity, the observed value of $V_{\rm bipolar}$ corresponds to a value of the mass to radius ratio of the compact object of $M/R \sim 40\ M_\odot/R_\odot$, *which is typical for a white dwarf.* Indeed, outflows with velocities of this order have been observed in cataclysmic variables (e.g. Drew 1991; Drew, Hoare & Woods 1991).

Since the value of M/R identifies the accreting object unambiguously as a white dwarf, we check further if the observed luminosity is consistent with a white dwarf burning hydrogen in a shell. For such an object, the luminosity is related to the white dwarf mass by (e.g. Iben & Tutukov 1989)

$$L/L_\odot \simeq 4.6 \times 10^4 (M_{\rm WD}/M_\odot - 0.26). \qquad (1)$$

Note that this relation differs somewhat from the usual Paczyński-Uus relation (Paczyński 1970; Uus 1970) which is appropriate for AGB stars which have both hydrogen and helium burning shells. The bolometric luminosity of 0513–69 is probably between $9.5 \times 10^{37}\,{\rm erg\,s^{-1}}$ (obtained from an LTE model atmosphere fit; Reinsch et al. 1996) and $2 \times 10^{38}\,{\rm erg\,s^{-1}}$ (obtained assuming a black body fit; Schaeidt, Hasinger & Trümper 1993). Using Eqn. 1 with these values gives a mass of $\sim 0.8 - 1.4\,M_\odot$, again consistent with a white dwarf.

From the above discussion we therefore conclude that the compact object in 0513–69 is almost certainly a white dwarf.

5.2. The Accretion Rate

Much of the optical luminosity of the system is probably generated in the accretion disk (although some fraction may represent the effects of nuclear burning and of illumination of the accretion disk and the secondary star by the hot white dwarf). For a distance modulus of 18.5 to the LMC and $E_{B-V} = 0.1$ (e.g. Panagia et al. 1991), we obtain (in the optical high states) $M_V \simeq -2$. *If* we assume that the entire luminosity comes from a standard accretion disk then, using the fact that the luminosity of the accretion disk is given approximately by (Webbink et al. 1987)

$$M_V^{\rm disk} \simeq -9.48 - \frac{5}{3}\log\left(\frac{M_{\rm WD}}{M_\odot}\frac{\dot{M}}{M_\odot {\rm yr}^{-1}}\right) - \frac{5}{2}\log\left(2\cos i\right) . \qquad (2)$$

where $\dot{M}$ is the accretion rate and i is the inclination angle, we obtain for $M_{\rm WD} = 1M_\odot$ and $i \simeq 10^\circ$ (see § 4.2), an accretion rate of $\dot{M} \simeq 10^{-5}M_\odot$ yr^{-1}. This accretion rate is of the order of the Eddington value, and it indicates that at least some fraction of the optical light is due to illumination (and perhaps nuclear burning on the white dwarf surface). It probably remains true, however, that the accretion rate in this system is extremely high. Another indication of the fact that the accretion rate in 0513–69 may be higher than in other similar systems (e.g. CAL 83) comes from the observation of the bipolar outflow (§ 2.2 and § 5.1). Typically, the mass flux in jets is of the order of 1–30% of the disk accretion rate (e.g. Lizano et al. 1988), and while not all the objects which exhibit jets have luminosities near the Eddington limit (although SS 433 does), it is certainly the case that the intermittent nature of the jets in young stellar objects seems to be associated with episodes of an increased accretion rate through the disk (e.g. Reipurth & Heathcote 1993).

The observed drops in the optical luminosity, by ~ 0.8 mag (§ 3), if interpreted as a reduction in the accretion rate, correspond to a decrease in $\dot{M}$ by a factor ~ 3. We should note, however, that if the optical luminosity is actually dominated by reprocessed radiation from the accretion disk and/or the secondary star, both being irradiated by the steady burning white dwarf, then the decrease in $\dot{M}$ could be by a larger factor. Such occasional drops in the accretion rate are observed in many nova-like variables and in particular in the group of cataclysmic variables known as VY Scl stars (e.g. Shafter 1992; Robinson et al. 1981; Honeycutt 1995). Similarly to the case of 0513–69, the downward transitions in VY Scl stars also occur on a timescale of tens of days (e.g. Hudec, Huth & Fuhrmann 1984; Liller 1980; Rosino, Romano & Marziani 1993; Honeycutt 1995).

Further evidence for the relation between the bipolar outflows and the accretion rate may be inferred from comparison of spectroscopic observations obtained during both high and low states. Optical spectroscopy obtained during a low state in December 1993 (C96; Reinsch et al. 1996) revealed the equivalent widths of the emission lines to be significantly weaker than in high state observations.

We shall return to the question of what can cause the drops in the mass transfer rate when

we discuss a comprehensive model for the system in § 5.4 below.

5.3. The Cause of the X-ray Outbursts

There are four main ways in which an accreting white dwarf can exhibit transient X-ray outbursts: (i) the outbursts may represent some phases in thermonuclear flashes occurring when a critical mass for ignition is accumulated (e.g. Iben 1982; Prialnik & Kovetz 1995), examples of this behaviour being provided by classical novae; (ii) the X-ray outbursts may be the consequence of a photospheric contraction during a nuclear shell burning phase (even if the burning was steady; e.g. MacDonald, Fujimoto & Truran 1985; Ögelman et al. 1993; Krautter et al. 1996); again, this behaviour has been observed in some nova systems; (iii) the X-ray luminosity may be generated in shocks resulting from the interaction of an ejected shell with the ISM; (iv) the outbursts may simply represent epochs in which the X-ray source is not shielded by intervening material (e.g. Pakull 1996).

Examining the X-ray data *alone* it is difficult to rule out regular thermonuclear flashes as a possible cause for the recurrent X-ray outbursts (this was, in fact, the model proposed by Kahabka 1995). However, when the X-ray data are examined *together* with the optical data, flashes caused by the accumulation of a critical mass become extremely unlikely. The reason is simply the fact that the second and the third X-ray outbursts observed in the system in July 1993 and in December 1994 occurred *during optical minima* (see Fig. 3), while *no outbursts were observed during optical high states* (Schaeidt 1996; Pakull et al. 1993). If this represents the rule (rather than being an accident), then it is very difficult to reconcile with a thermonuclear flash model, which is normally accompanied by radius expansion and an increased optical luminosity (see e.g. Livio 1994 for a discussion). Even if a thermonuclear flash was able to produce a decrease in the optical luminosity (for example, if it led only to a modest expansion, but which nevertheless managed to destroy the disk), this would *follow* the X-ray rise, contrary to what is probably observed (see § 5.4 and Fig. 3). We may thus rule out the thermonuclear flash model. The shock emission model ((iii) above) may also be eliminated as a possible source for the increase in the X-rays, since the ejection of a shell is normally a consequence of significant expansion (e.g. Prialnik & Kovetz 1995).

We are therefore left with the episodic unveiling of a permanent X-ray source or contraction during a steady shell burning phase as the most probable origins for the increase in the X-ray luminosity (see Pakull et al. 1993; Pakull 1996). In the former model, the white dwarf is burning steadily all the time, but is visible (in X-rays) only during phases of low mass transfer rate (see § 5.4 for a possible cause of such phases). At other times, the wind and bipolar outflow are optically thick to soft X-rays. It should be noted that the decrease in the optical should precede the rise in the X-rays, which is probably consistent with the available data (see § 5.4).

We may investigate whether the outflow can indeed shield the source using the following

simplified approximation. If we assume a spherical outflow, characterised by a velocity law of the type $V = V_\infty (1 - R_{\rm WD}/r)^\beta$, where V_∞ is the outflow velocity at a large distance, then we can calculate the optical depth in the outflow,

$$\tau = \frac{\sigma}{4\pi m_p V_\infty R_{\rm WD}} f(X,\beta)\dot{M}_{\rm outflow}. \qquad (3)$$

Here, m_p is the proton mass, σ is the absorption cross-section to the soft X-rays, $\dot{M}_{\rm outflow}$ is the mass outflow rate and $f(X,\beta)$ is a function of $X \equiv R_{\rm WD}/R_{\rm S}$, where $R_{\rm S}$ is the sonic radius in the outflow and β is the exponent in the velocity law. For values of β in the range $1.0 - 4.5$ and $X \sim 1/50$, both typical for nova-like variables (e.g. Knigge 1995), $f(X,\beta) \sim 0.02$. If we use, for example, the photoelectric absorption cross-section at $0.28 - 0.40$ keV from Morrison & McCammon (1983), $V_\infty \sim 4000$ km s^{-1}, and $R_{\rm WD} \sim 10^9$ cm, we obtain that the source will be totally obscured ($\tau \sim 5$) for $\dot{M}_{\rm outflow} \gtrsim 3 \times 10^{-9} M_\odot$ yr^{-1}. This number should not be taken as representing the real value, since the actual obscuration depends crucially on the geometry of the real outflow from the accretion disk (e.g. Knigge, Woods & Drew 1995), especially in a nearly pole-on system.

Whilst the above discussion does indicate that a scenario of this type is, in principle, viable, we find the white dwarf photospheric contraction model more reasonable; this is discussed fully in § 5.4 below. It is important to note that the appearance of a relatively short lived X-ray phase due to contraction of the photosphere, during shell burning, has been established observationally for both GQ Mus (Ögelman et al. 1993; Shanley et al. 1995) and V1974 Cyg (Krautter et al. 1996). This puts us now in a position where we can attempt to propose a comprehensive model for the system, taking all the available observational data into consideration.

5.4. A Comprehensive Model of Photospheric Contraction

The principal features of the photospheric contraction model which emerge as a result of the discussion in the previous sections are the following. The system consists of a white dwarf which may be fairly massive (both because of the constraints imposed by the accretion luminosity, see § 5.2, and by the inclination angle, § 4.2; see also below), which accretes from an *evolved* companion.

The accretion rate is normally very high (perhaps $\sim 10^{-6} M_\odot$ yr^{-1}), at a value which is near the top of the steady burning strip in the $\dot{M} - M_{WD}$ plane (e.g. Nomoto 1982). Under these conditions, the white dwarf is slightly inflated (by perhaps no more than a factor ~ 3 in radius; Kovetz & Prialnik 1994), and most of the shell luminosity is probably emitted in the UV. The mass transfer rate, and concomitantly the optical luminosity, suffer occasional drops by about a factor 3 or more. This is a very similar phenomenon to the one exhibited by VY Scl stars and some nova-like variables (e.g. Honeycutt 1995; Honeycutt, Robertson & Turner 1995).

The important point here is that 0513–69, like the VY Scl stars, experiences only *downward*

transitions. Livio & Pringle (1994) suggested a model for VY Scl stars, in which the reduced mass transfer rate is a consequence of a magnetic spot covering the L_1 region. VY Scl stars are normally found in the period range 3–4 hrs and in the Livio & Pringle model, this is a consequence of the fact that when the rotation rate of the star (which is coupled to the orbit) increases, so does the magnetic activity and the fraction of the stellar surface covered with spots (e.g. Kürster et al. 1992). One may therefore wonder why the secondary in 0513–69, which has an orbital period of $\sim$ 0.76 d, should exhibit a similar behaviour. However, it should be remembered that the secondary in 0513–69 is evolved. The physical quantity which characterizes the magnetic activity is the Rossby number, $P_{\rm rot}/\tau_{\rm C}$, where $\tau_{\rm C}$ is the convective overturn time in the envelope (e.g. Schrijver 1994). Since evolved stars have deeper convective envelopes (longer $\tau_{\rm C}$) than main sequence stars, they exhibit the same level of activity at longer $P_{\rm rot}$ (see e.g. Schrijver 1994 for a review). In fact, the orbital period of 0513-69 is close to the range spanned by the magnetically active RS CVn stars.

Once the accretion rate drops, the photosphere contracts slightly (e.g. Kovetz & Prialnik 1994; Kato 1985), raising the effective temperature and thus producing an increase in the X-ray luminosity. It is important to note in this respect that the decrease in the optical luminosity, *precedes* the rise in the X-rays. Fig. 3 shows the times at which the X-rays were known to be off (arrows marked "XX") and on (arrows marked "X"), in relation to the optical behaviour. Using the fact that the X-ray rise time is of order 6 days (Schaeidt 1996 - see also § 1), we may be fairly confident that, at least in the X-ray outburst of December 1994 (day number $\sim$ 1715 in Fig. 3), the optical had already started to fall before the X-rays turned on. In this respect, the episodic unveiling model (discussed in § 5.3 above) is also consistent with the available data. However, Reinsch et al. (1996) have shown that the optical low states of 0513–69 are accompanied by a reddening of $\sim$ 0.1 mags, which is quantitatively consistent with the decreased disk illumination resulting from a contraction in the white dwarf radius.

Furthermore, the photospheric contraction model is able to provide a natural explanation of details in the light curve morphology, as described below. The increased X-ray flux irradiates the companion star and, either by inflating material above the secondary's photosphere and causing it to be transferred (e.g. Ritter 1988), or by heating the magnetic spot area (which is generally cooler, e.g. Parker 1979), causes the mass transfer rate to increase again. This produces the step-like behaviour of the optical light curve when the luminosity increases, or the small jump in the optical luminosity in the middle of the low state (around day 1539, Fig. 3). The following should also be noted: in *all* cases, the luminosity immediately following the end of one of these low states is slightly higher than the average between these events (see Fig. 3). This is entirely consistent with the above model, since the temporary blocking of the mass transfer (e.g. by a magnetic spot), plus the effect of the irradiation of the secondary by the X-rays, is likely to result in a somewhat increased mass transfer rate, once the blocking is removed.

A question which needs to be addressed is whether the contraction and expansion of the white dwarf photosphere can occur on the observed timescale ($\sim$ 1 week). An examination of the

results of Kovetz & Prialnik (1994) and Kato (1996) reveals that this is indeed possible, if the white dwarf is massive ($M_{\rm WD} \sim 1.3 - 1.4\ M_{\odot}$). This can be easily understood if we realise that the contraction timescale can be reasonably approximated by the duration of the mass-ejection phase (Livio 1992):

$$\tau_{\rm duration} \simeq \xi \left(\frac{M_{\rm WD}}{M_{\rm C}}\right)^{-1} \left[\left(\frac{M_{\rm WD}}{M_{\rm C}}\right)^{-2/3} - \left(\frac{M_{\rm WD}}{M_{\rm C}}\right)^{2/3}\right]^{3/2}, \qquad (4)$$

where ξ is nearly a constant and $M_{\rm C}$ is the Chandrasekhar mass. Using a value for $\xi \approx 51$ days, which fits the observations of 84 novae in M31 and 15 novae in the LMC (Della Valle & Livio 1995), gives a contraction timescale of less than 4 days for a $1.3 M_{\odot}$ white dwarf.

Assuming that the main ingredients of the model outlined above are correct, we may ask what is the cause for the difference in the X-ray behaviour of 0513–69 and similar sources (such as CAL 83). The main difference is probably in the ratio of the mean mass transfer rate to the rate at which steady burning occurs (for the given white dwarf mass). This ratio is probably higher for 0513-69, a hypothesis which is supported by the greater optical luminosity of this system ($V_{\rm mean} \sim 16.8$ in the high states, compared with $V_{\rm mean} \sim 17.3$ for CAL 83; Cowley et al. 1993). Evidence for a high mass transfer rate is provided both by the brightness of the accretion disk, and by the fact that a bipolar outflow is not observed in CAL 83 (C96).

Finally, we should point out that the main model discussed in the present work (§ 5.4) is based on the probable observation that the rise in X-rays came *after* the optical luminosity was observed to drop. Thus, it can be tested directly by long-term monitoring of the system in the optical and X-ray regimes. In particular, the model predicts that increases in the X-ray luminosity should follow drops (by ~ 1 mag) in the optical luminosity. If future observations will show that this is indisputably the case, then the model of photospheric contraction will be further strengthened.

We are grateful to the MACHO collaboration for allowing us access to their long term photometry of 0513–69. We thank the staff at the AAT, Siding Spring, for their assistance with the spectroscopic observations. KAS acknowledges the hospitality of ST ScI, and support from PPARC. ML acknowledges support from NASA Grants NAGW 2678 and GO-4377. We are grateful to Paul Schmidtke and Anne Cowley for providing us with information about their observations, and to the anonymous referees for their detailed comments.

Table 1. Journal of observations.

Date (m/d/y)	HJD−2440000	Exposure (s)	Wavelength coverage (Å)
11/29/94	9686.214	1000	4367−5070
11/29/94	9686.226	1000	"
11/29/94	9686.237	600	6103−6857
11/29/94	9686.245	600	"
11/29/94	9686.253	600	"
11/30/94	9687.023	1800	4367−5070
11/30/94	9687.039	855	"
12/1/94	9688.019	1800	"
12/1/94	9688.070	1800	"
12/1/94	9688.093	1800	"
12/1/94	9688.115	1800	"
12/1/94	9688.139	1800	"
12/1/94	9688.161	1800	"

Table 2. Mean equivalent widths of emission features (Å)

Line	Night 1	Night 2	Night 3	Overall average
HeII 4541	1.2±0.3	1.5±0.2	1.1±0.1	1.4±0.1
HeII 4686	20.7±0.8	19.2±0.5	20.6±0.2	20.4±0.2
S^{-}_{4686}	0.9±0.3	0.5±0.2	0.9±0.1	0.8±0.1
S^{+}_{4686}	0.3±0.3	1.0±0.2	1.1±0.1	1.1±0.1
$H\beta$	13.2±0.6	11.3±0.4	10.7±0.2	10.8±0.1
$S^{-}_{H\beta}$	0.1±0.3	0.0±0.2	0.2±0.1	0.2±0.1
$S^{+}_{H\beta}$	1.3±0.4	0.8±0.3	1.4±0.1	1.3±0.1
$H\alpha$	48.2±1.4	-	-	48.2±1.4
$S^{-}_{H\alpha}$	1.6±0.6	-	-	1.6±0.6
$S^{+}_{H\alpha}$	2.6±0.7	-	-	2.6±0.7

Table 3. Approximate wavelengths and relative velocities of Doppler-shifted components.

Line	λ_0 (Å)	S^- (Å)	S^+ (Å)	S^- (km s^{-1})	S^+ (km s^{-1})
HeII 4686	4691	4631	4752	3850	3900
Hβ	4866	4806	4932	3700	4050
Hα	6569	6488	6657	3700	4000

Table 4. Radial velocities of HeII 4686.

Spectrum no.	HJD−2440000	Velocity (km s^{-1})
1	9686.214	291±5
2	9686.226	272±7
3	9687.023	288±3
4	9687.039	293±10
5	9688.019	313±7
6	9688.070	312±3
7	9688.093	311±2
8	9688.115	312±5
9	9688.139	309±2
10	9688.161	307±3

REFERENCES

Alcock, C. et al. 1995, Phys. Rev. Lett., 74, 2867

Alcock, C. et al. 1996, MNRAS, in press

Blandford, R. 1993, Astrophysical Jets, eds. D. Burgarella, M. Livio, & C. O'Dea (Cambridge: Cambridge University), p. 15

Cowley, A. P., Schmidtke, P. C., Hutchings, J. B., Crampton, D. & McGrath, T. K. 1993, ApJ, 418, L63

Cowley, A. P., Schmidtke, P. C., Crampton, D., & Hutchings, J. B. 1996, in IAU Symp. 165, Compact Stars in Binaries, eds. E. P. J. van den Heuvel & van Paradijs (Dordrecht: Kluwer), p. 439

Crampton, D., Hutchings, J. B., Cowley, A. P., Schmidtke, P. C., McGrath, T. K. O'Donoghue, D., & Harrop-Allin, M. K. 1996, ApJ, 456, 320 (C96)

Della Valle, M. & Livio, M. 1995, ApJ, 452, 704

Drew, J. E. 1991, in Structure and Emission Properties of Accretion Disks, eds. C. Bertout et al. (Gif sur Yvette: Editions Frontieres), p. 331

Drew, J. E., Hoare, M. G., & Woods, J. A. 1991, MNRAS, 250, 144

Hasinger, G. 1994, Rev. Mod. Astr., 7, 129

Hjellming, R. M. & Rupen, M. P. 1995, Nature, 375, 464

Honeycutt, R. K. 1995, private communication

Honeycutt, R. K., Robertson, J. W., & Turner, G. W. 1995, in Cataclysmic Variables, eds. A. Bianchini et al. (Dordrecht: Kluwer), p. 75

Horne, K. 1986, PASP, 98, 609

Hudec, R., Huth, H., & Fuhrmann, B. 1984, Observatory, 104, 1

Iben, I. Jr. & Tutukov, A. V. 1989, ApJ, 342, 430

Iben, I. Jr. 1982, ApJ, 259, 244

Kahabka, P. 1995, A&A, 304, 227

Kahabka, P. & Trümper, J. 1996, in IAU Symp. 165, Compact Stars in Binaries, eds. E. P. J. van den Heuvel & J. van Paradijs (Dordrecht: Kluwer), p. 425

Kato, M. 1985, PASJ, 37, 19

Kato, M. 1996, in Supersoft X-ray Sources, Lecture Notes in Physics, ed. J. Greiner, (Springer Verlag), in press

Knigge, C. 1995, D.Phil. thesis, Oxford University

Knigge, C., Woods, J. A. & Drew, J. E. 1995, MNRAS, 273, 225

Kovetz, A. & Prialnik, D. 1994, ApJ, 424, 319

Krautter, J., Ögelman, H., Starrfield, S., Wichmann, R. & Pfeffermann, E. 1996, ApJ, 456, 788

Kürster, M., Hatzes, A. P., Pallavicini, R., & Randich, S. 1992, in Cool Stars, Stellar Systems and the Sun, ASP Conf. Ser., 26, eds. M. S. Giampapa & J. A. Bookbinder (San Francisco: ASP), p. 249

Liller, M. H. 1980, AJ, 85, 1092

Livio, M. 1992, ApJ, 393, 516

Livio, M. 1994, in Interacting Binaries, eds. H. Nussbaumer & A. Orr (Berlin: Springer-Verlag), p. 135

Livio, M. & Pringle, J. E. 1994, ApJ, 427, 956

Lizano, S., Heiles, C., Rodriguez, L. F., Koo, B.-C., Shu, F. H., Hasegawa, T., Hayashi, S., & Mirabel, I. F. 1988, ApJ, 328, 763

MacDonald, J., Fujimoto, M. Y., & Truran, J. W. 1985, ApJ, 294, 263

Mirabel, I. F. & Rodriguez, L. F. 1994, Nature, 371, 46

Morrison, R. & Mc Cammon, D. 1983, ApJ, 270, 119

Nomoto, K. 1982, ApJ, 253, 798

Ögelman, H., Orio, M., Krautter, J., & Starrfield, S. 1993, Nature, 361, 331

Paczyński, B. 1970, Acta. Astron., 20, 47

Pakull, M. W., Motch, C., Bianchi, L., Thomas, H.-C., Guilbert, J., Beaulieu, J. P., Grison, P., & Schaeidt, S. 1993, A&A, 278, L39

Pakull, M. W. 1994, private communication

Pakull, M. W. 1996, in Supersoft X-ray Sources, Lecture Notes in Physics, ed. J. Greiner, (Springer Verlag), in press

Panagia, N., Gilmozzi, R., Macchetto, F., Adorf, H.-M., & Kirshner, R. P. 1991, ApJ, 380, L23

Parker, E. N. 1979, Cosmical Magnetic Fields (Oxford: Clarendon)

Prialnik, D. & Kovetz, A. 1995, ApJ, 445, 789

Rappaport, S., Di Stefano, R., & Smith, J. D. 1994, ApJ, 426, 692

Reinsch, K., van Teeseling, A., Beuermann, K. & Abbott, T. M. C. 1996, A&A, in press

Reipurth, B. & Heathcote, S. 1993, in Astrophysical Jets, eds. D. Burgarella, M. Livio, & C. O'Dea (Cambridge: Cambridge University Press), p. 35

Ritter, H. 1988, A&A, 202, 93

Roberts, D. H., Léhar, J. & Dreher, J. W. 1987, AJ, 93, 968

Robinson, E. L., Barker, E. S., Cochran, A. L., Cochran, W. D., & Nather, R. E. 1981, ApJ, 251, 611

Rosino, L., Romano, G., & Marziani, P. 1993, PASP, 105, 51

Scargle, J. D., 1982, ApJ, 263, 835

Schaeidt, S., Hasinger, G., & Trümper, J. 1993, A&A, 270, L9

Schaeidt, S. 1996, in Supersoft X-ray Sources, Lecture Notes in Physics, ed. J. Greiner, (Springer Verlag), in press

Schandl, S., Meyer-Hofmeister, E. & Meyer, F., 1996, A&A, submitted

Schmidtke, P. C., McGrath, T. K., Cowley, A. P. & Frattare, L. M. 1993, PASP, 105, 863

Schrijver, C. J. 1994, in Cool Stars, Stellar Systems and the Sun, ASP Conf. Ser., 64, ed. J.-P. Caillault (San Francisco: ASP), p. 328

Shafter, A. W. 1992, ApJ, 394, 268

Shanley, L., Ögelman, H., Gallagher, J. S., Orio, M., & Krautter, J. 1995, ApJ, 438, L95

Uus, U. 1970, Nauch. Inf., 17, 32

van den Heuvel, E. P. J., Bhattacharya, D., Nomoto, K., & Rappaport, S. A. 1992, A&A, 262, 97

Vermeulen, R. 1993, in Astrophysical Jets, eds. D. Burgarella, M. Livio, & C. O'Dea (Cambridge: Cambridge University), p. 241

Webbink, R. F., Livio, M., Truran, J. W., & Orio, M. 1987, ApJ, 314, 653

Yungelson, L., Livio, M., Truran, J. W., Tutukov, A., & Fedorova, A., 1995, ApJ, submitted

This preprint was prepared with the AAS LaTeX macros v4.0.

Fig. 1.— Average blue spectrum of 0513–69. The resolution is ~ 1.3 Å. The principal HeII and H emission features are marked, along with their associated Doppler-shifted components (see § 2.2). Note the extended blue wing of HeII 4686 and lack of blue emission in Hβ.

Fig. 2.— Average red spectrum of 0513–69. The resolution is ~ 1.3 Å. The spectrum is dominated by Hα, but Doppler-shifted S^+/S^- components are just discernable above the noise.

Fig. 3.— The optical light curve of 0513–69 from 1992 Aug. 22 – 1995 Nov. 27. These observations were obtained as a by-product of the MACHO project (see Alcock et al. 1996). The relative magnitude is shown for the "blue" filter, which is approximately equivalent to the Johnson V passband. Note the quasi-regular magnitude drops of ~ 1 mag. The symbol "SAAO" around day no. 1754 indicates the time at which we obtained our fast optical photometry (see § 3.1). Downward and upward vertical arrows indicate the times at which the system was known to be on (X) and off (NX) in X-rays respectively (see § 1, § 5.3 and § 5.4).

Fig. 4.— White light photometry of 0513–69 relative to a local standard (upper curve). The magnitude of a comparison star relative to the same local standard is also plotted (lower curve). 0513–69 shows a significant fading of ~ 0.1 mags over the duration of the observations (220 mins).

Fig. 5.— Triple Gaussian fit (solid curve) to the HeII 4686 average profile (dash-dotted line). The components consist of a narrow function to fit the line core, and 2 broad, low-amplitude Gaussians which fit the red and blue sections of the extended profile base.

Fig. 6.— CLEANED periodogram for HeII 4686 radial velocity data (using 10 iterations and a loop gain of 0.1). The frequency range is $\nu = 0.1 - 10.0$ cycles d^{-1}, and the search increment used is $\Delta\nu = 0.001$ cycles d^{-1}. The most power arises at P$= 0.761 \pm 0.025$ d, with a one day^{-1} alias at $\nu = 0.22$ cycles d^{-1}

Fig. 7.— The CLEANED periodogram for our HeII 4686 velocity data and the radial velocities of C96 (using 10 iterations and a loop gain of 0.1). The most power arises at P$= 0.761 \pm 0.004$ d; one day^{-1} aliases are also present.

Fig. 8.— The radial velocity curve obtained by folding our HeII 4686 data on an orbital period of P$= 0.76278 \pm 0.00005$ d, using the photometric ephemeris of Alcock et al. (1996). Phase zero corresponds to maximum optical light. The parameters of the sinusoidal fit are K$= 14.5 \pm 3$ km s^{-1}, $\gamma = 297 \pm 1$ km s^{-1} and $o_o = 0.17 \pm 0.09$. Two cycles are plotted for clarity.

Fig. 9.— The component mass parameter space for a mass function of 0.0002 and inclinations of $3 - 15°$. If the accreting star is a white dwarf, the system must be observed nearly pole-on.

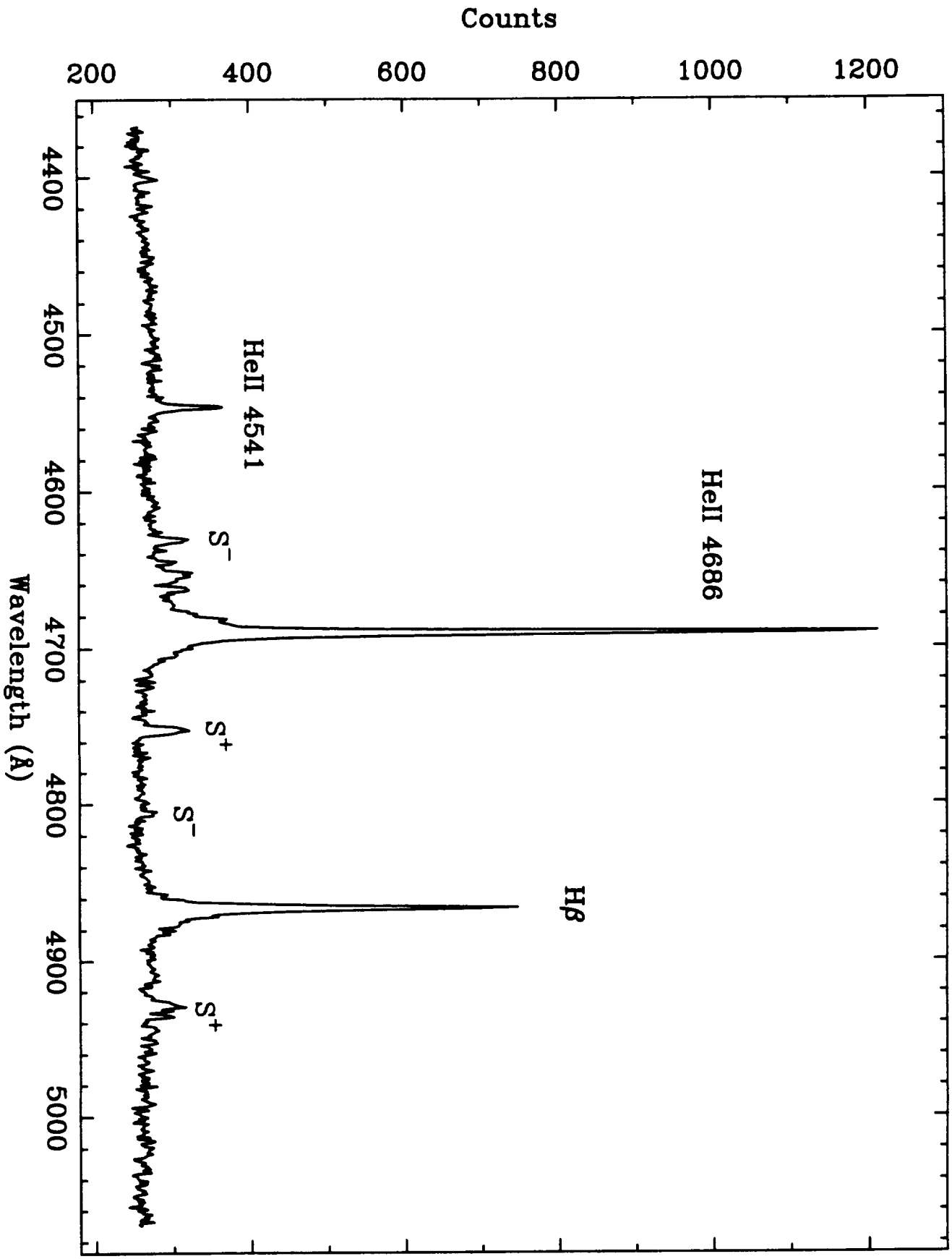
Counts
200
400
600
800
1000
1200
Wavelength (Å)
4400
4500
4600
4700
4800
4900
5000
HeII 4541
S−
HeII 4686
S+
S−
Hβ
S+

Figure 1

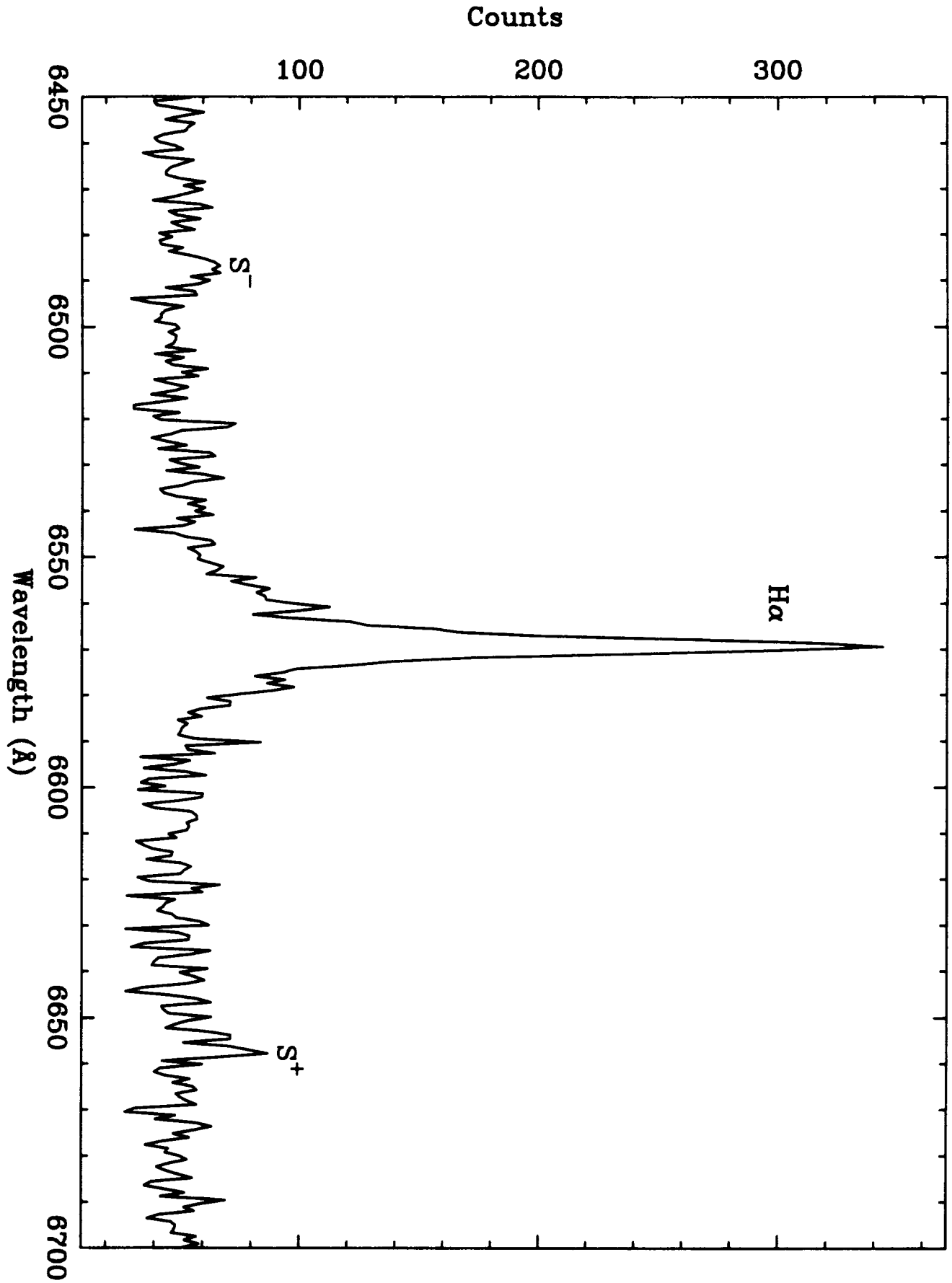
Counts
100
200
300
6450
6500
6550
6600
6650
6700
Wavelength (Å)
S-
Hα
S+

Figure 2

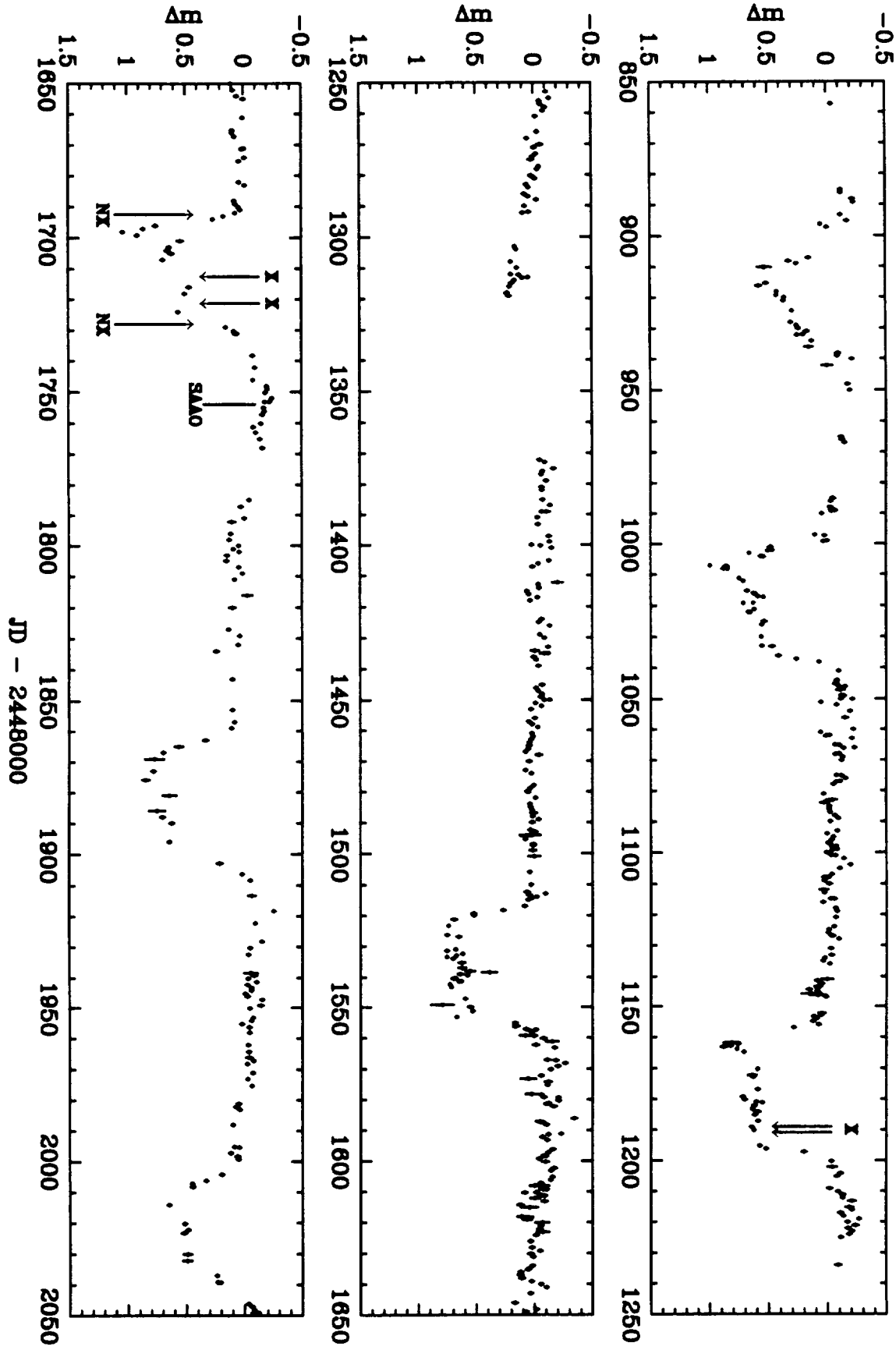

Figure 3

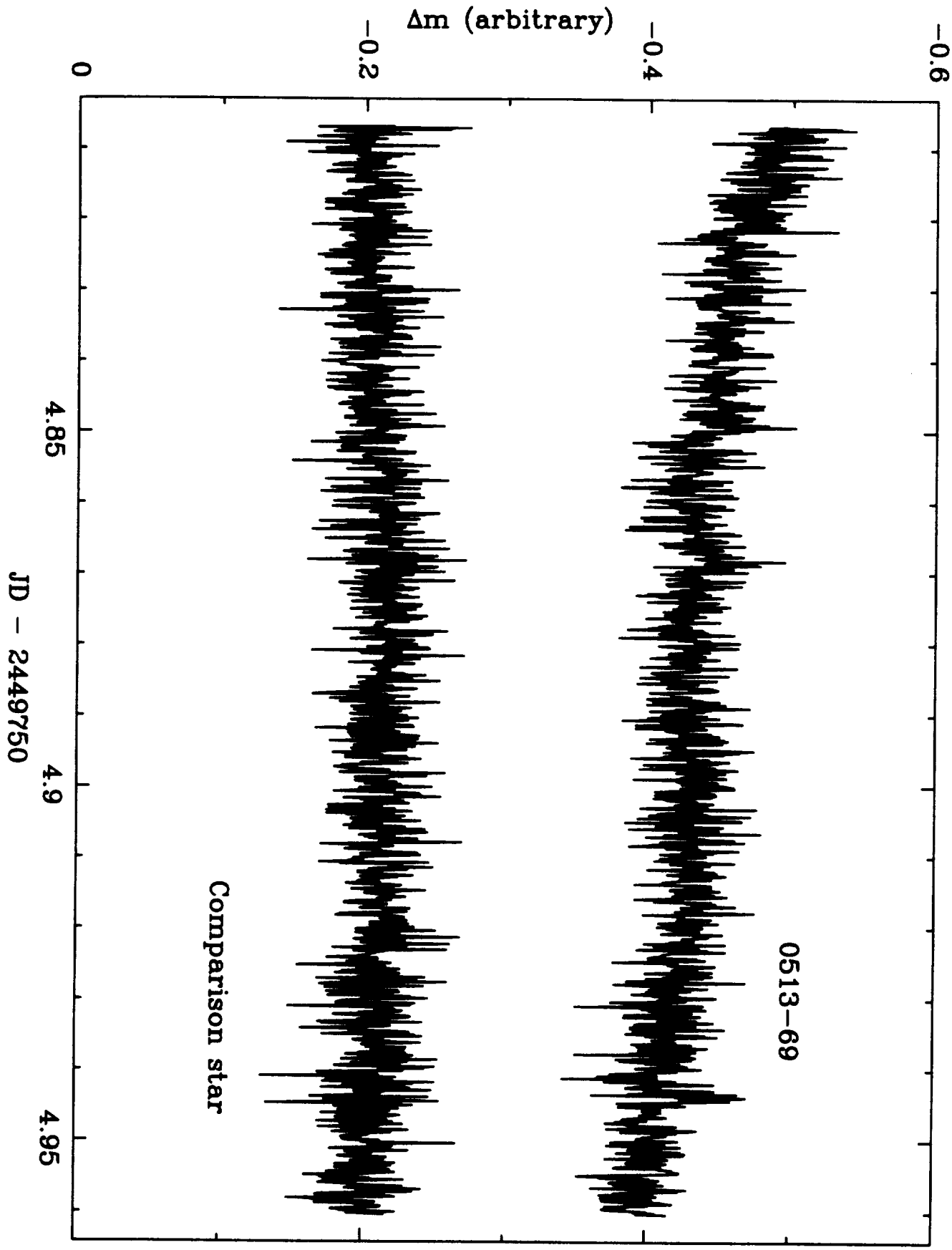
Δm (arbitrary)
0
−0.2
−0.4
−0.6
4.85
4.9
4.95
JD − 2449750
Comparison star
0513−69

Figure 4

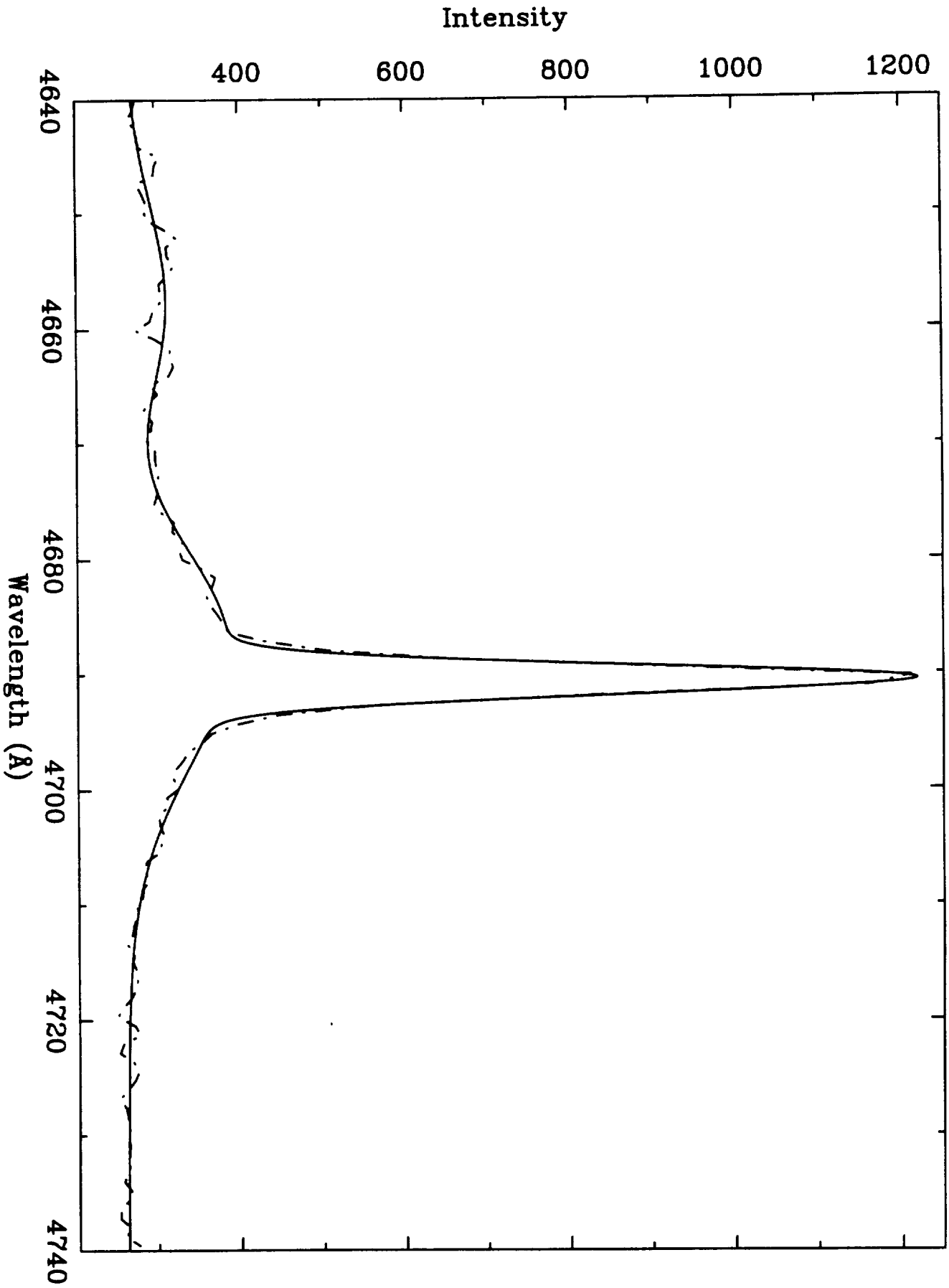
Intensity
400
600
800
1000
1200
4640
4660
4680
4700
4720
4740
Wavelength (Å)

Figure 5

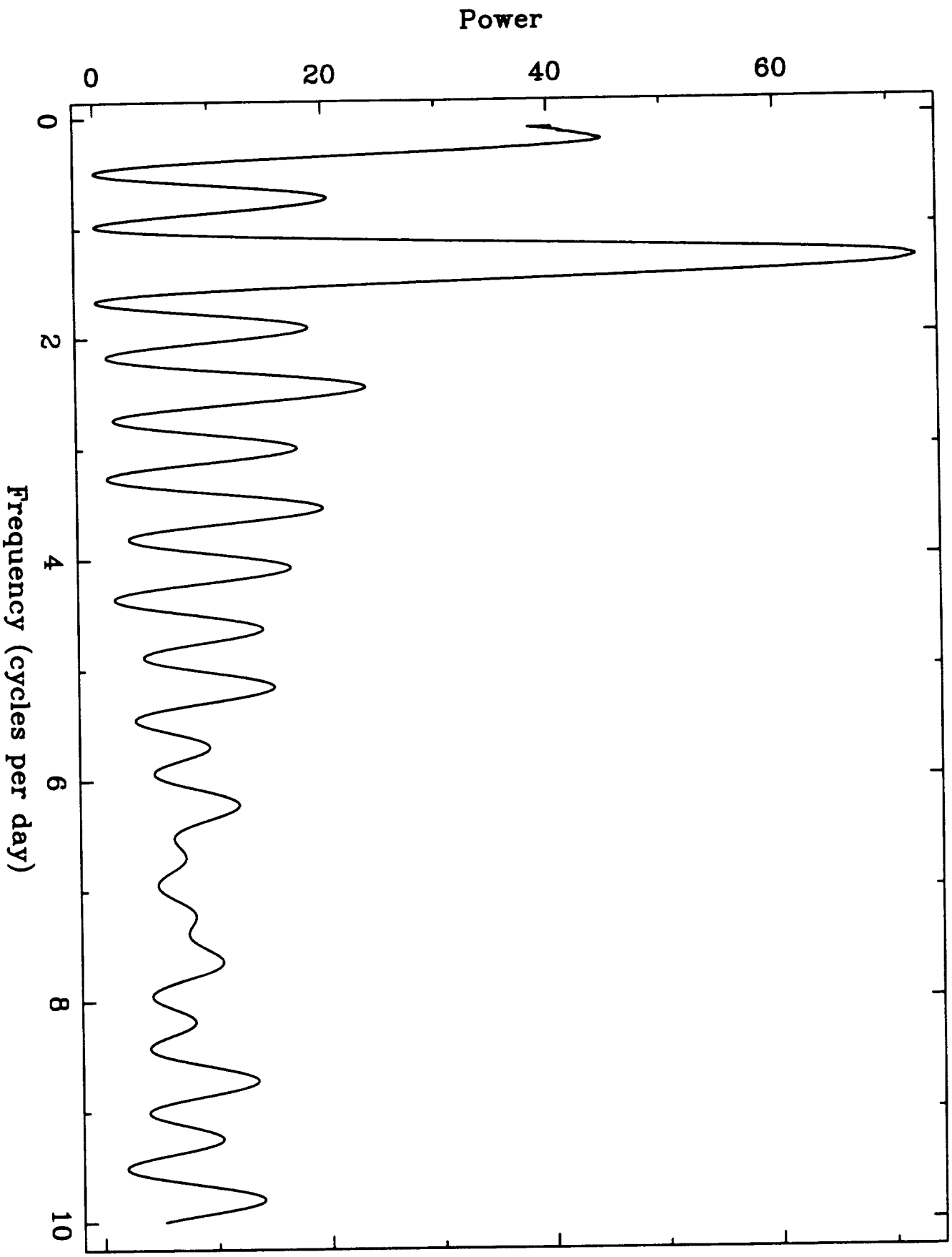

Figure 6

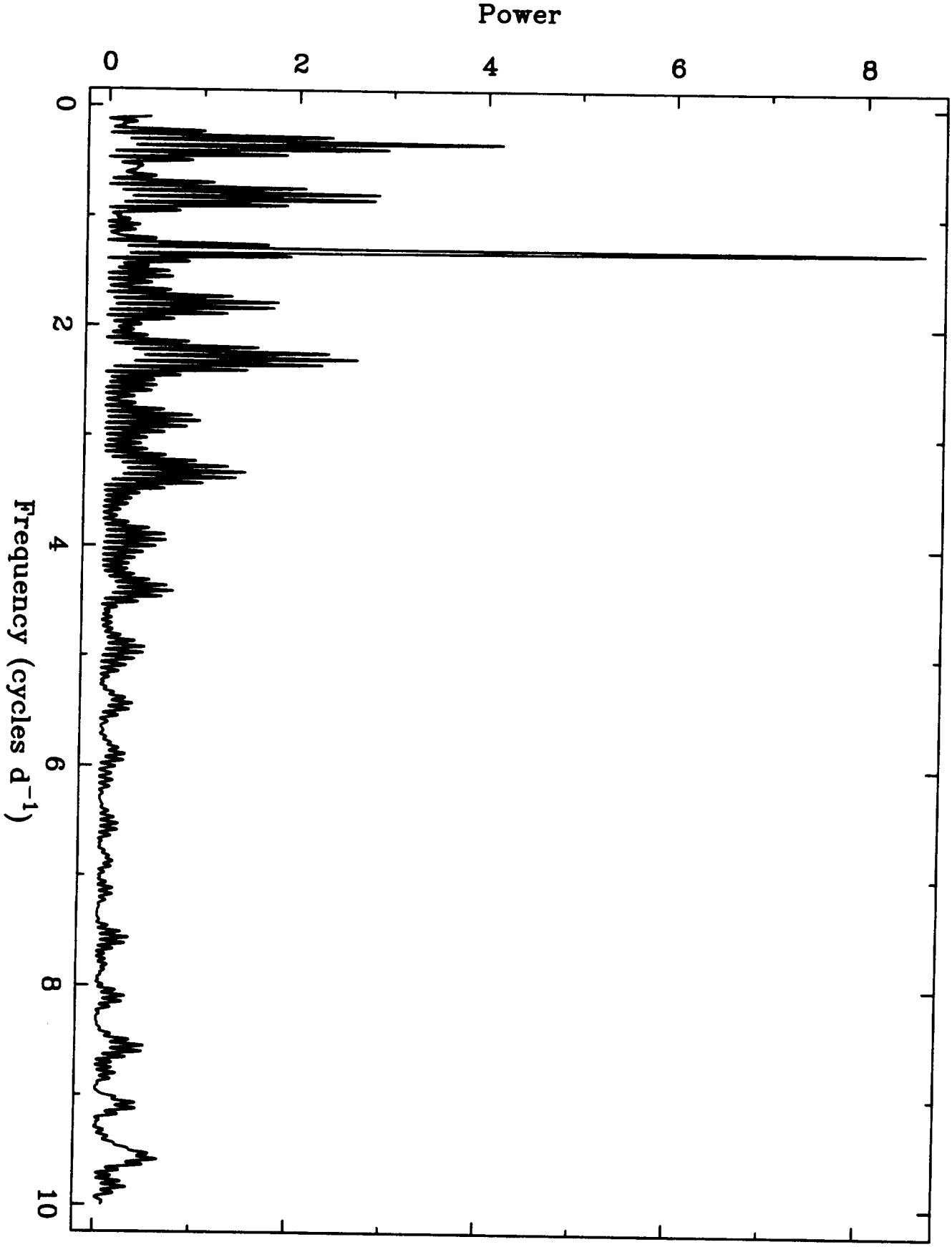

Figure 7

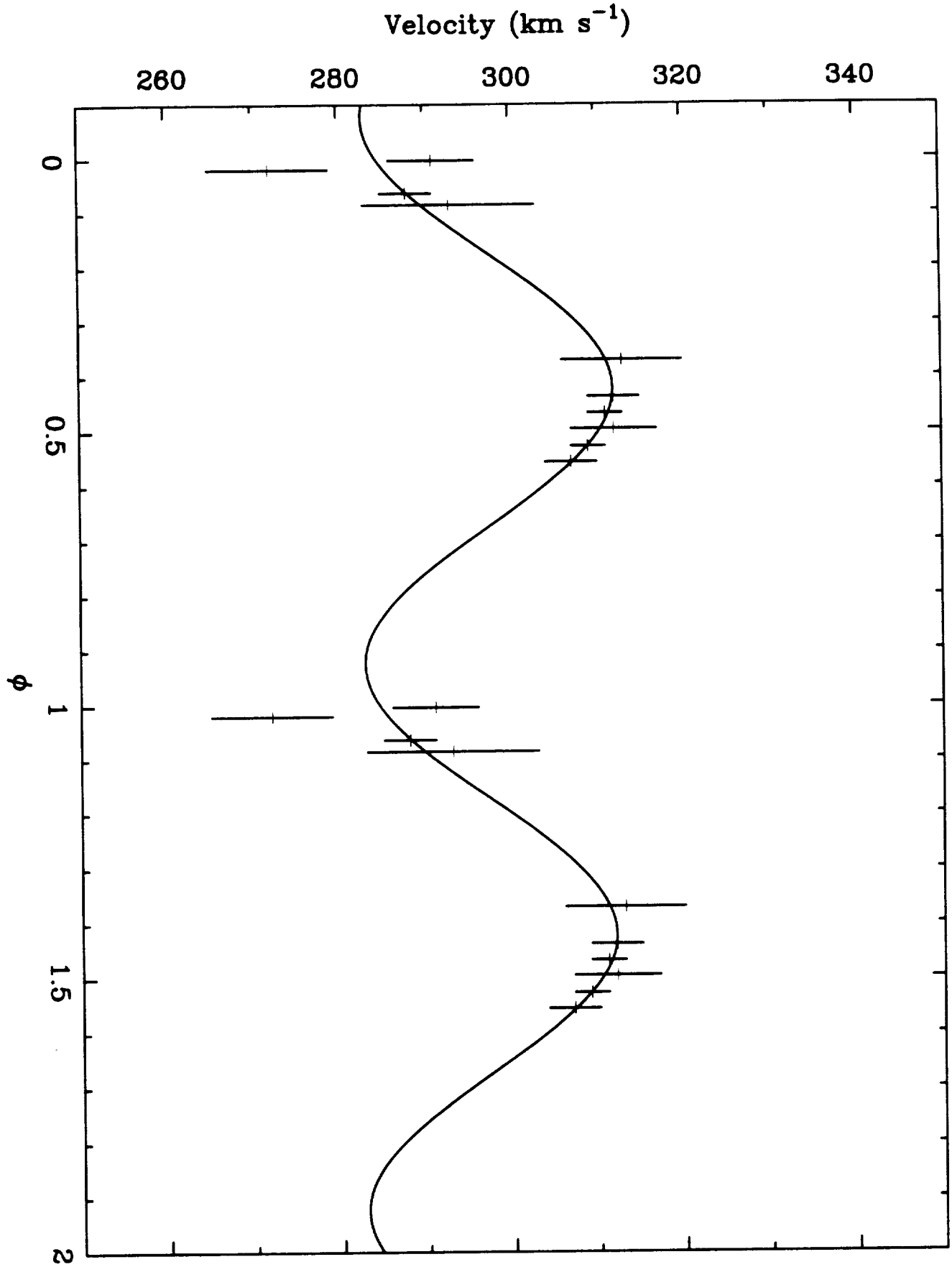

Figure 8

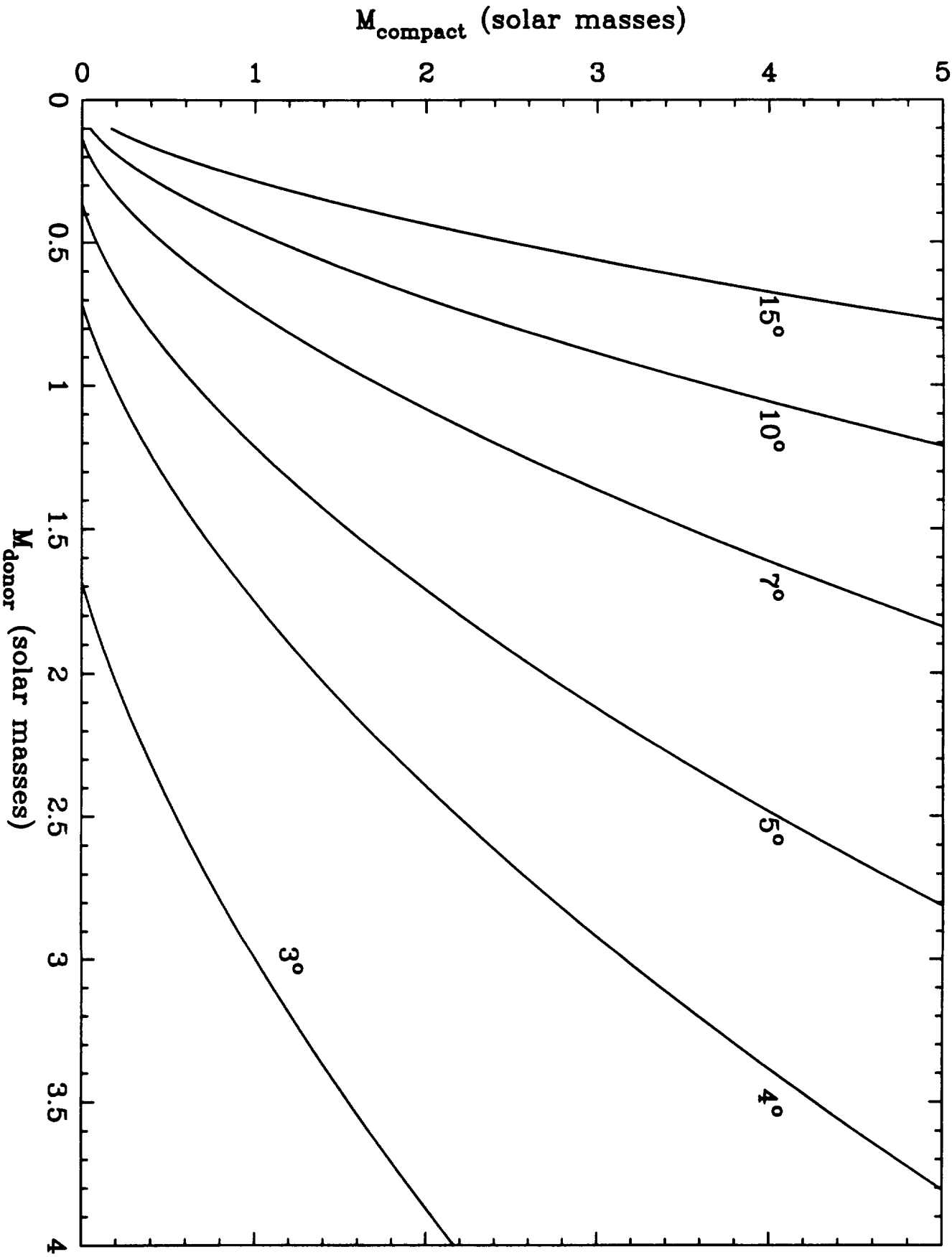
M_compact (solar masses)
0
1
2
3
4
5
M_donor (solar masses)
0
0.5
1
1.5
2
2.5
3
3.5
4
15°
10°
7°
5°
4°
3°

Figure 9